Supplementary information

Appendix: Radiomic features

Table A1. Extracted tumor morphologic features

Morphologic features	Qualitative description	Mathematical description
Volume	Tumor volume (in mm^3)	$Total\ number\ of\ voxels$
Perimeter	Tumor perimeter (in mm)	$\sum_{i}^{n} \sqrt{\Delta x^2 + \Delta y^2}$
Eccentricity	Tumor regularity. The quality of fit of an ellipse to the tumor shape [36].	$\frac{\sum_i \frac{\sqrt{(x_e - x_i)^2 + (y_e - y_i)^2}}{\sqrt{(x_i - x_c)^2 + (y_i - y_c)^2}}}{n}$
Roundness	Tumor roundness	$\frac{Area\ of\ a\ shape}{Area\ of\ circle}$
Equivalent spherical radius	Radius of a sphere of an equivalent volume	$\sqrt[3]{\left(\frac{3}{4}\right) V/\pi}$

n represents the total number of vertices (x_i, y_i) in the closed polygon. $\Delta x = x_{i+1} - x_i$ and $\Delta y = y_{i+1} - y_{i..}$ An ellipse fit to the closed polygon shape has coordinates (x_e, y_e).

Table A2. Extracted structural texture features

Structural feature	Qualitative description	Mathematical description
Local Binary Pattern (LBP)	Intensity variation between a pixel and its neighboring pixels[38,39].	$LBP\ (x_c,\ y_c) = \sum_{p=0}^{P-1} q(I_p - I_c)2^P,\ (x_p, y_p)$ $= [x_c + Qcos\left(\frac{2\pi p}{P}\right), y_c$ $- Qsin\left(\frac{2\pi p}{P}\right)]$ I_c and I_p are gray-level intensity values for pixel (x_c,y_c) and pixel (x_p,y_p). q: indicator function, 0 for negative inputs and 1 for non-negative inputs Q, P: parameters to set pixel neighborhood size, set to 1 and 8, respectively[39,40].

Table A3. Extracted run-length texture features

Run-length features	Qualitative description	Mathematical description
Short run emphasis (SRE)	Emphasis on short runs	$1/n_r \sum_{i=1}^{M}\sum_{j=1}^{N} \frac{(R(i,j))}{j^2}$
Long run emphasis (LRE)	Emphasis on long runs	$1/n_r \sum_{i=1}^{M}\sum_{j=1}^{N} \big(R(i,j)\big) * j^2$
Gray level nonuniformity (GLN)	Degree of gray-level run dissimilarity	$1/n_r \sum_{i=1}^{M}(\sum_{j=1}^{N} R(i,j))^2$
Run length nonuniformity (RLN)	Dissimilarity in length of runs	$1/n_r \sum_{j=1}^{N}(\sum_{i=1}^{M} R(i,j))^2$
Run percentage (RP)	Distribution of runs	$\frac{n_r}{\#pixels}$
Low gray level run emphasis (LGRE)	Emphasis on low-gray-level values	$1/n_r \sum_{i=1}^{M}\sum_{j=1}^{N} \frac{\big(R(i,j)\big)}{(i+j)^2}$
High gray level run emphasis (HGRE)	Emphasis on high-gray-level values	$1/n_r \sum_{i=1}^{M}\sum_{j=1}^{N} \big(R(i,j)\big) * i^2$
Short run low gray level emphasis (SRLGE)	Emphasis on short runs with low-gray-level values	$1/n_r \sum_{i=1}^{M}\sum_{j=1}^{N} \frac{\big(R(i,j)\big)}{j^2(i+j)^2}$
Short run high gray level emphasis (SRHGE)	Emphasis on short runs with low-gray-level values	$1/n_r \sum_{i=1}^{M}\sum_{j=1}^{N} \frac{\big(R(i,j)\big)(i+j)^2}{j^2}$
Long run low gray level emphasis (LRLGE)	Emphasis on long runs with low-gray-level values	$1/n_r \sum_{i=1}^{M}\sum_{j=1}^{N} \frac{\big(R(i,j)\big)j^2}{(i+j)^2}$
Long run high gray level emphasis (LRHGE)	Emphasis on long runs with low-gray-level values	$1/n_r \sum_{i=1}^{M}\sum_{j=1}^{N} \big(R(i,j)\big)(i+j)^2$

nr is the total number of runs, R(*i*,*j*) represents the number of runs with pixels of gray-level intensity value, *i*, and length of run, *j*. 128 gray-levels were used. Estimated by averaging over 0°, 45°, 90°, and 135° orientations.

Table A4. Extracted gray-level co-occurrence matrix texture features

Co-occurrence matrix features	Qualitative description	Mathematical description
Contrast	Intensity contrast between pixel and its neighbor	$\sum_{ij} \lvert i-j \rvert^2 f(i,j)$
Correlation	Linear gray-level dependence	$\sum_{ij} \frac{\left((i-\mu_i) * \left(j-\mu_j\right) * f(i,j)\right)}{\sigma_i \sigma_j}$
Homogeneity	Closeness of distribution in co-occurrence matrix to matrix diagonal	$\sum_{ij} \frac{f(i,j)}{1+\lvert i-j \rvert}$
Energy	Certainty of gray-level co-occurrence	$\sum_{ij} f(i,j)^2$
Entropy	Uncertainty of gray-level co-occurrence	$-\sum_{ij} f(i,j) * \log\left(f(i,j)\right)$
Inverse Difference Moment (IDM)	Local homogeneity in gray-level co-occurrence	$\sum_{ij} \frac{f(i,j)}{(1+(i-j)^2)}$
Cluster Shade	Asymmetry in gray-level values	$\sum_{ij} \left(i-\mu_i+j-\mu_j\right)^3 * f(i,j)$

Table A5. Extracted gray-level histogram texture features

Gray-level histogram features	Qualitative description	Mathematical description
Mean	Mean gray-level value	$\sum_k \frac{k * g(k)}{\sum_k g(k)}$
Median	Median gray-level value	Median(K)
Min	Min gray-level value	Min(*k)*
Max	Max gray-level value	Max(*k)*
Interquartile range	Interquartile range of gray	$P_{75} - P_{25}$
5th Percentile	Histogram bin that 5% of gray level values are less than or equal to	k: 5% of values ≤ *k*
Mean 5th	Mean value of gray-level values that 5% of gray level values are less than or equal to	$\frac{\sum_k k*g(k)}{\sum_k g(k)}$ for $k \leq$ fifth percentile
10^{h} Percentile	Histogram bin that 10% of gray level values are less than or equal to	k: 10% of values ≤ *k*
25th Percentile	Histogram bin that 25% of gray level values are less than or equal to	k: 25% of values ≤ *k*
75th Percentile	Histogram bin that 75% of gray level values are less than or equal to	k: 75% of values ≤ *k*
95th Percentile	Histogram bin that 95% of gray level values are greater than or equal to	k: 95% of values ≥ *k*

Mean 95th	Mean value of gray-level values that 95% of gray level values are greater than or equal to	$\frac{\sum_k k*g(k)}{\sum_k g(k)}$ for $k \geq$ ninety- fifth percentile
Sum	Sum of gray-level values	$\sum_k k * g(k)$
Standard deviation	Measure of variation of gray-level values around the mean	$\sqrt{\sum_k (k-\mu)^2 * g(k)}$
Entropy	Measure of histogram nonuniformity	$-\sum_k g(k) * \log(g(k))$
Kurtosis	Measure of histogram flatness	$\sigma^{-4} \sum_k (k-\mu)^4 * g(k) - 3$
Skewness	Measure of histogram symmetry	$\sigma^{-3} \sum_k (k-\mu)^3 * g(k)$
Uniformity	Measure of histogram uniformity	$\Sigma_k g(k)^2$

Table A6. Extracted gray-level size zone matrix texture features

Size zone matrix features	Qualitative description	Mathematical description
Gray level mean	Measure of mean gray level intensities for zones	$\Sigma_{i=1}^{N_g}\Sigma_{j=1}^{N_z} i\, p_{ij}$
Gray level non-uniformity	Measure of the variability of gray-level intensity values	$\frac{1}{N_s}\,\Sigma_{i=1}^{N_g} s^2$
Gray level variance	Measure of the variance in gray level intensities for the zones	$\Sigma_{i=1}^{N_g}\Sigma_{j=1}^{N_z}(i-\mu)^2\, p_{ij}$
High gray level emphasis	Measure of the distribution of high gray level values	$\frac{1}{N_s}\,\Sigma_{i=1}^{N_g} s_i i^2$
Large zone emphasis	Measure of larger zone sizes	$\frac{1}{N_s}\,\Sigma_{j=1}^{N_z} s_j j^2$
Large zone high gray level emphasis	Measure of the distributions of larger zone sizes with higher gray level values	$\frac{1}{N_s}\,\Sigma_{i=1}^{N_g}\Sigma_{j=1}^{N_z} i^2 j^2 s_{ij}$
Large zone low gray level emphasis	Measure of the distributions of larger zone sizes with lower gray level values	$\frac{1}{N_s}\,\Sigma_{i=1}^{N_g}\Sigma_{j=1}^{N_z} \frac{j^2 s_{ij}}{i^2}$
Low gray level emphasis	Measure of the distribution of low gray level values	$\frac{1}{N_s}\,\Sigma_{i=1}^{N_g} \frac{S_i}{i^2}$

Small zone emphasis	Measure of smaller zone sizes	$\frac{1}{N_s} \Sigma_{j=1}^{N_z} \frac{s_j}{j^2}$
Small zone high gray level emphasis	Measure of the distributions of smaller zone sizes with higher gray level values	$\frac{1}{N_s} \Sigma_{i=1}^{N_g} \Sigma_{j=1}^{N_z} \frac{i^2 s_{ij}}{j^2}$
Small zone low gray level emphasis	Measure of the distributions of smaller zone sizes with lower gray level values	$\frac{1}{N_s} \Sigma_{i=1}^{N_g} \Sigma_{j=1}^{N_z} \frac{s_{ij}}{i^2 j^2}$
Zone percentage	Ratio between the number of zones and number of voxels	$\frac{N_s}{N_v}$
Zone size entropy	Entropy of zone sizes	$-\Sigma_{i=1}^{N_g} \Sigma_{j=1}^{N_z} p_{ij} \log_2 p_{ij}$
Zone size mean	Mean zone size in the image	$\Sigma_{i=1}^{N_g} \Sigma_{j=1}^{N_z} j \, p_{ij}$
Zone size non-uniformity	Measure of variability of zone size volumes in the image	$\frac{1}{N_s} \Sigma_{j=1}^{N_z} s^2 j$

Zone size variance	$\Sigma_{i=1}^{N_g}\Sigma_{j=1}^{N_z}(j-\mu)^2\ p_{ij}$

N_g is the number of discretized gray levels present in the image, N_z is the maximum zone size of any group of linked voxels. N_s is the total number of zones and N_v is the total number of voxels. S_{ij} is the number of zones with discretized gray level, *i* , and size, *j*.

Supplemental figure 1. Summary of patient characteristics from validation cohort. Statistical comparison between discovery and validation cohorts for covariates common in the two datasets.

Supplemental figure 2. Radiomic analysis workflow. 3-D tumor region is automatically segmented from the DCE-MRI scans (A). Signal enhancement ratio (SER) generated using first and second post-contrast DCE-MRI scans (B). Morphologic and texture based radiomic features extracted from the SER map (C).

Supplemental figure 3. Representative cases from heterogeneity phenotypes. Representative slice, tumor region, and SER map from a pre-menopausal woman diagnosed with primary stage-I, HR+, HER2- , node-negative breast cancer assigned to the low heterogeneity phenotype (top), a peri-menopausal woman with primary stage-II, HR-, HER2+, node- negative breast cancer assigned to the medium heterogeneity phenotype (middle), and a pre-menopausal woman with primary stage-II, ER-, HER2-, node-positive breast cancer assigned to the high heterogeneity phenotype (bottom).

Supplemental figure 4. Independent validation of intrinsic imaging phenotypes of tumor heterogeneity. Phenotypes identified in the discovery cohort are significantly reproducible in the validation cohort (A). RFS curves for women stratified by imaging heterogeneity phenotype show that heterogeneity phenotype is statistically significant ($p = 0.01$) when predicting RFS (B).

a

	Non-recurrent cases 119 (73% of total)	**Recurrent cases 44 (27% of total)**	Significance tested using Chi-square analysis
Receptor status			**p=0.07**
Hormone receptor positive	67 (56%)	25 (56%)	
HER2 positive	34 (29%)	18 (40%)	
Triple Negative	29 (24%)	10 (23%)	

b

	Discovery n=95	**Validation** n= 163	Significance tested using Chi-square analysis
Recurrent cases	11 (12%)	44 (27%)	**p = 0.02**
Receptor Status			
Hormone receptor positive	70 (74%)	92 (56%)	**p = 0.02**
HER2 positive	22 (23%)	52 (32%)	**P=0.3**
Triple Negative	12 (13%)	39 (24%)	**p=0.4**
Clinical stage			**p < 0.001**
Early stage (1)	36 (38%)	0 (0%)	
Advanced Stage (2-3)	55 (58%)	163 (100%)	

Supplemental figure 1. Summary of patient characteristics from validation cohort. Statistical comparison between discovery and validation cohorts for covariates common in the two datasets.

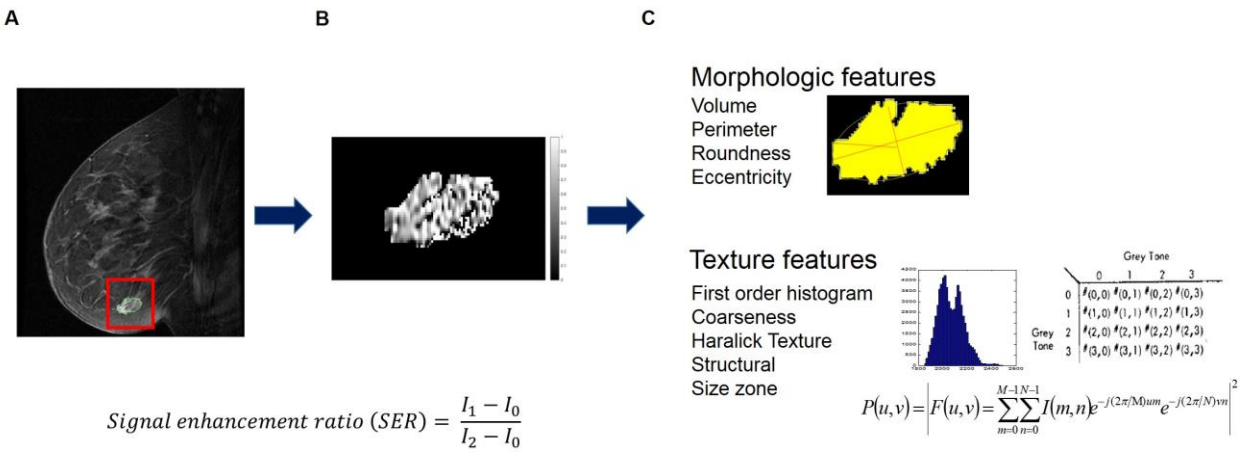

Supplemental figure 2. Radiomic analysis workflow. 3-D tumor region is automatically segmented from the DCE-MRI scans (A). Signal enhancement ratio (SER) generated using first and second post-contrast DCE-MRI scans (B). Morphologic and texture based radiomic features extracted from the SER map (C).

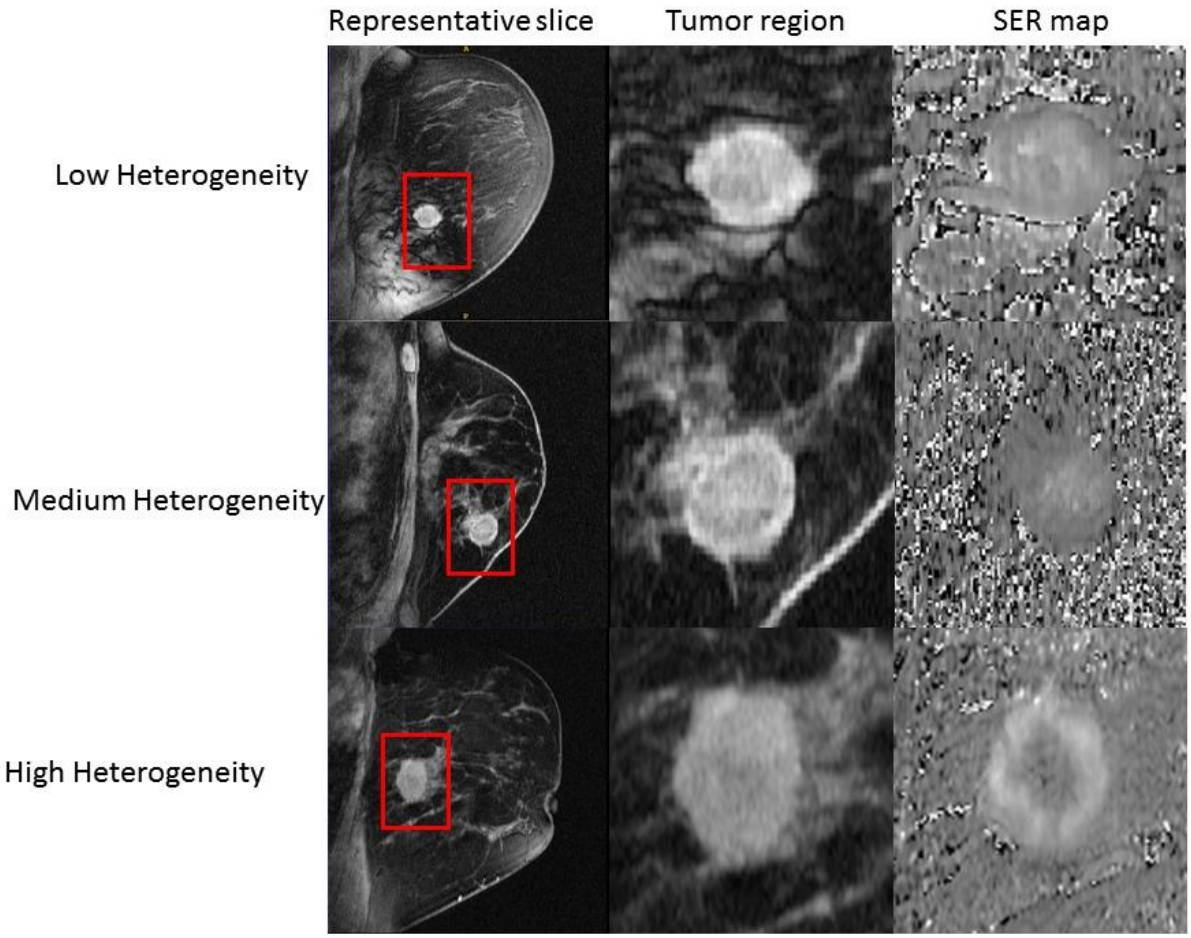

Supplemental figure 3. Representative cases from heterogeneity phenotypes. Representative slice, tumor region, and SER map from a pre-menopausal woman diagnosed with primary stage-I, HR+, HER2- , node-negative breast cancer assigned to the low heterogeneity phenotype (top), a peri-menopausal woman with primary stage-II, HR-, HER2+, node- negative breast cancer assigned to the medium heterogeneity phenotype (middle), and a pre-menopausal woman with primary stage-II, ER-, HER2-, node-positive breast cancer assigned to the high heterogeneity phenotype (bottom).

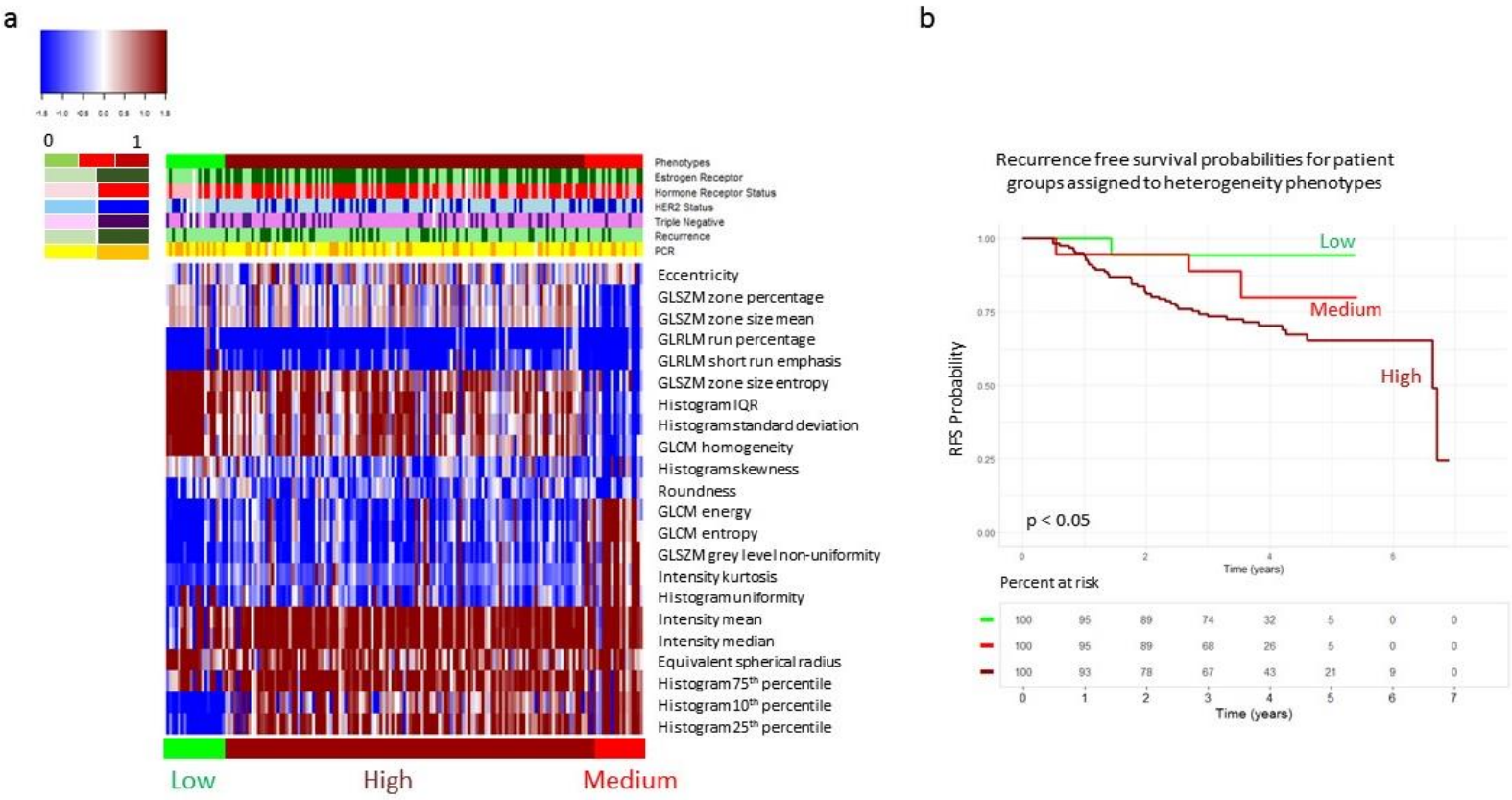

Supplemental figure 4. Independent validation of intrinsic imaging phenotypes of tumor heterogeneity. Phenotypes identified in the discovery cohort are significantly reproducible in the validation cohort (A). RFS curves for women stratified by imaging heterogeneity phenotype show that heterogeneity phenotype is statistically significant ($p = 0.01$) when predicting RFS (B).